Revealing the effects of defect states on the nonlinear absorption properties of TlInSSe and $Tl_2In_2S_3Se$ crystals in near-infrared optical limiting applications

Anıl Doğan[a], Ahmet Karatay[a,*], Mehmet Isik[b,c,d], Elif Akhüseyin Yıldız[a], Nizami Mamed Gasanly[e,f], Ayhan Elmali[a]

[a]*Department of Engineering Physics, Faculty of Engineering, Ankara University, 06100, Ankara, Türkiye*
[b]*Department of Electrical and Electronics Engineering, Atilim University, 06836 Ankara, Türkiye*
[c]*Department of Biomedical Engineering, Faculty of Engineering and Architecture, İzmir Bakırçay University, 35665, Izmir, Türkiye*
[d]*Biomedical Technologies Design Application and Research Center, İzmir Bakırçay University, 35665, Izmir, Türkiye*
[e]*Department of Physics, Science and Art Faculty, Middle East Technical University, 06800 Ankara, Türkiye*
[f]*Virtual International Scientific Research Centre, Baku State University, 1148 Baku, Azerbaijan*

ABSTRACT

Present study represents the effect of defect states on the nonlinear absorption and optical limiting performances of TlInSSe and $Tl_2In_2S_3Se$ single crystals with near-infrared excitations. The band gap energies are 2.2 and 2.22 eV and the Urbach energies are 0.049 and 0.034 eV for TlInSSe and $Tl_2In_2S_3Se$, respectively. The trapping time of localized defect states is found as 8 ns by femtosecond transient absorption measurements. The analysis of open aperture Z-scan data depends on two different fitting models to determine the effect of defect states on the nonlinear absorption (NA) properties of the studied crystals. Model 1 only considers two-photon absorption (TPA), while model 2 includes one-photon absorption (OPA), TPA and free carrier absorption (FCA). The NA coefficients (β_{eff}) obtained from model 2 are higher than the values (β) obtained from model 1 at same intensities reveals that defect states contribute to NA through OPA. The optical limiting properties of TlInSSe and $Tl_2In_2S_3Se$ crystals were examined at 1064 nm wavelength excitations. The limiting thresholds were found to be 1.16 mJ/cm^2 and 0.27 mJ/cm^2 at 29.8 GW/m^2 and 99.5 GW/m^2 input intensities, respectively. The results show that TlInSSe and $Tl_2In_2S_3Se$ crystals have promising potential for near-infrared optical limiting applications.

Keywords: TlInSSe crystal, $Tl_2In_2S_3Se$ crystal, Defect states, Nonlinear absorption, Optical limiting.

Published by CRYSTAL GROWTH & DESIGN
https://doi.org/10.1021/acs.cgd.4c00606

1. INTRODUCTION

Chalcogenide materials have wide usage areas such as solar cells [1, 2], supercapacitors [3], sensors [4-6], optical limiting [7], ovonic threshold switch (OTS) selectors [8], photocatalysis [9], energy storage [10], infrared-imaging [11], spintronics [12], and water splitting [13]. Moreover, crystal forms of chalcogenide materials have a significant role in certain optoelectronic applications such as optical signal processing, imaging, biomedical sensing, gas detection, and light detection and ranging (LIDAR) due to their infrared transmissions, adjustable refractive index, mid-infrared nonlinear optical properties, and low phonon energies [14-17] . Among the chalcogenide crystals, the TlInSeS crystal is a layered structured semiconductor material formed by replacing half of the sulfur atoms of the $TlInS_2$ compound with selenide atoms [18]. Thallium dichalcogenides are a family of crystals with the chemical formula $TlBX_2$, where B can be In or Ga, and X can be S, Se, or Te [19, 20]. This group includes both layered structures (such as $TlGaS_2$, $TlGaSe_2$, and $TlInS_2$) and chain structures (such as $TlInSe_2$, $TlInTe_2$, and $TlGaTe_2$). $TlInS_2$, a layered crystal within this family, belongs to the monoclinic system with a space group of C_{2h}^6. It serves as a chemical analog to TlSe, featuring a univalent thallium atom and a trivalent In atom. The lattice is composed of two-dimensional layers arranged periodically, with each subsequent layer rotated by 90° relative to the one below it. Interlayer bonds are formed between Tl and S atoms, while intralayer bonds are formed between In and S atoms. The ac plane view of the crystal structure, with the a-axis oriented in the [110] direction, is depicted in the inset of Fig. 1, showing the layered arrangement [21]. The primary structural component of each layer is the In_4S_6 adamantane-like unit, connected by bridging S atoms. These units combine to form layers with trigonal prismatic voids that house Tl atoms, which align into nearly planar chains along the [110] and [110] directions. $TlInS_2$ and $TlInSe_2$ crystals have potential in various application areas such as photovoltaics [22], electrical switching [23], and dilute magnetic semiconductors [24]. Additionally, TlS_2 and $TlSe_2$-based materials combined with In and Ga show two-photon absorption (TPA) properties, which are important for optical power limiting applications [25-27]. The temperature-dependent optical properties, electrical and dielectric properties, structural analysis, and nonlinear optical characterizations of TlInSeS crystals are available in the literature. The band gap energy of the TlInSeS crystal is about 2.2 eV. Therefore, it is a proper semiconductor material for near-infrared nonlinear optical applications [18, 28, 29].

The nonlinear optical response of semiconductor material to high-intensity light is a useful property for various applications such as photodetection [30], ultrafast solid-state laser [31-33], self-frequency doubling [34], optical limiting [35], and optical switching [36]. In the presence of

sufficiently high-intensity light, the nonlinear response can occur in the form of nonlinear absorption (NA) corresponding to a decrease in the transmittance by absorbing light via one-photon absorption (OPA) [37-39], TPA [40-46], or free-carrier absorption (FCA) [47], or in the form of saturable absorption (SA) [48] which results in an increase in the transmittance due to the filling of excited states by electrons. For protecting the human eye and detectors from irreversible damage of high-intensity light the properties of materials to limit the light passing through them via NA are investigated [49-52]. While the optical limiter allows light to pass up to a certain intensity, it prevents the passage of light above this intensity.

This study has two strategies. The first is to reveal the effect of defect states on nonlinear absorption through OPA. By introducing this effect, the nonlinear absorption performance can be tuned using the defect state density. For this purpose, nonlinear adsorption performances were investigated according to model 1 containing only TPA and model 2 containing OPA and TPA. The second aim is to investigate the optical limiting performance in the NIR and IR regions. Optical limiting is attracting more attention, especially in the NIR and IR regions, in terms of defense industry applications. Studies on the examination of nonlinear absorption properties of various chalcogenides are available in the literature [53-55]. However, the optical limiting properties of TlInSSe and $Tl_2In_2S_3Se$ crystals have not been determined, although their nonlinear absorption is in the NIR region. Considering all this information, our study aims to examine the nonlinear absorption and optical limiting properties of TlInSSe and $Tl_2In_2S_3Se$ crystals with the effects of defect states. Linear and optical characterization of TlInSSe and $Tl_2In_2S_3Se$ crystals was performed in the previous studies [29, 56]. Nonlinear absorption properties of TlInSSe and $Tl_2In_2S_3Se$ crystals are investigated under various intensities via open aperture (OA) Z-scan measurements with 4 ns pulsed laser excitations at 1064 nm.

2. EXPERIMENTAL PROCESSES

TlInSSe: $(TlInS_2)_{0.5}(TlInSe_2)_{0.5}$ and $Tl_2In_2S_3Se$: $(TlInS_2)_{0.75}(TlInSe_2)_{0.25}$ crystals were grown employing the Bridgman method. Thallium (Tl), Indium (In), Sulfur (S), and Selenium (Se) were used as raw materials throughout the growth process. All raw materials were of high purity, with Tl, In, S, and Se being 99.999% pure. The raw materials were mixed in a stoichiometric ratio corresponding to the formula of TlInSSe and $Tl_2In_2S_3Se$; specifically, Tl, In, S, and Se were combined in a 1:1:1:1 molar ratio for TlInSSe and 2:2:3:1 molar ratio for $Tl_2In_2S_3Se$. In this process, molten constituents were introduced into silica cylinders possessing a diameter of 10 mm and a length of 25 cm. The system was maintained under a vacuum of approximately 10^{-5} Torr, and the sealed ampule was incrementally translated at a rate of 1.0

mm per hour through a thermal gradient of 30 °C/cm. Subsequently, an X-ray diffraction analysis was conducted using a Rigaku Miniflex diffractometer, which utilized Cu-Kα radiation with a wavelength (λ) of 1.54 Å. The resulting crystalline ingots, exhibiting an orange hue, demonstrated favorable optical properties, and freshly cleaved surfaces exhibited a mirror-like quality. The chemical composition of the $Tl_2In_2S_3Se$ crystals was determined through Energy Dispersive Spectroscopic Analysis using a JSM-6400 Electron Microscope, as detailed in a prior publication [57]. The composition of the investigated samples (Tl : In : S : Se) was identified as 25.9 : 26.1 : 35.9 : 12.1, aligning well with the chemical formula of $Tl_2In_2S_3Se$.

The linear absorption properties of the studied crystals were investigated by a UV-VIS spectrophotometer (Shimadzu-1800). The charge transfer dynamics of the crystals were determined by performing ultrafast pump probe spectroscopy in femtosecond (fs) regime. The pump probe setup includes a Ti:Sapphire laser amplifier (Spectra Physics, Spitfire Pro XP, TOPAS) with 52 fs pulse duration and 1 kHz repetition rate. To set pump wavelength an optical parametric amplifier was used. The pulse duration of the laser source was determined as 120 fs by cross-correlation within the pump probe assembly. Pump wavelengths were determined depending on the maximum linear absorption wavelength of the crystals. The measurement of the excited state dynamics were performed between 0.1 picosecond (ps) and 3.2 nanosecond (ns) time scale with a white light continuum probe (Spectra Physics, Helios). Experimental results were analyzed by Surface Xplorer software (Ultrafast Systems). The nonlinear absorption properties of the crystals at various intensities were investigated through an open aperture (OA) Z-scan setup with 1064 nm wavelength Q-switched Nd:YAG laser source (Quantel Brilliant) at 4 ns pulse duration and 10 Hz repetition rate.

3. RESULTS AND DISCUSSIONS

3.1. Structural characterization

Figure 1 presents the X-ray diffraction (XRD) pattern obtained from the TlInSSe crystal. Within the angular range of 10-70^o, the XRD spectrum presents three distinct and well-defined peaks, located at approximately 23.70°, 47.20°, and 62.80°. The sharpness and clarity of these peaks signify the good crystalline quality of the grown TlInSSe compound. Notably, the positions of these observed peaks align with the characteristic data found in the standard reference (JCPDS No. 34-0097), reinforcing the fidelity of the crystal's structure. Furthermore, the Miller indices corresponding to these prominent peaks are thoughtfully provided directly above them. Upon scrutinizing the XRD pattern of the powdered form of the TlInSSe compound, the material's crystalline structure was discerned to be monoclinic [56].

In our recent paper [29] published with the aim of determining the crystal and optical properties of $Tl_2In_2S_3Se$ crystal, in which nonlinear absorption properties will be examined throughout this study, the x-ray diffraction pattern of the crystal was reported. Three distinct peaks were identified at angular positions of approximately 23.75°, 30.95°, and 48.50 associated with the monoclinic crystalline structure. The compound $Tl_2In_2S_3Se$ exhibits characteristics indicative of a layered semiconductor. Its structural framework bears resemblance to $TlInS_2$, albeit with a modification involving the substitution of one-quarter of the sulfur atoms with selenium atoms. The crystal structure of $Tl_2In_2S_3Se$ comprises alternating two-dimensional layers oriented parallel to the (001) plane [57]. Sequential layers are rotated by a 90° angle relative to their predecessors. Interlayer interactions manifest between Tl and S(Se) atoms, while intralayer bonds form between In and S(Se) atoms. Detailed crystallographic characteristics of $TlInS_xSe_{2-x}$ compounds was previously reported [58]. An analysis of the diffraction patterns revealed that two series of solid solutions are formed within the $TlInS_xSe_{2-x}$ system. The first series, $TlInSe_2$–$TlInS_{0.4}Se_{1.6}$, is dominated by $TlInSe_2$, which has a tetragonal structure and belongs to space group D_{4h}^{18}. The second series, $TlInS_{0.6}Se_{1.4}$–$TlInS_2$, is dominated by $TlInS_2$, characterized by a monoclinic structure and belonging to space group C_{2h}^{6}. The boundary between these two series occurs at approximately x ~ 0.5. According to this study the lattice constants of TlInSSe (x = 1) and $Tl_2In_2S_3Se$ (x = 1.5) were around a = 10.94 Å, b = 10.98 Å, c = 15.28 Å, β = 100.5° and a = 10.92 Å, b = 10.96 Å, c = 15.22 Å, β = 100.3°, respectively.

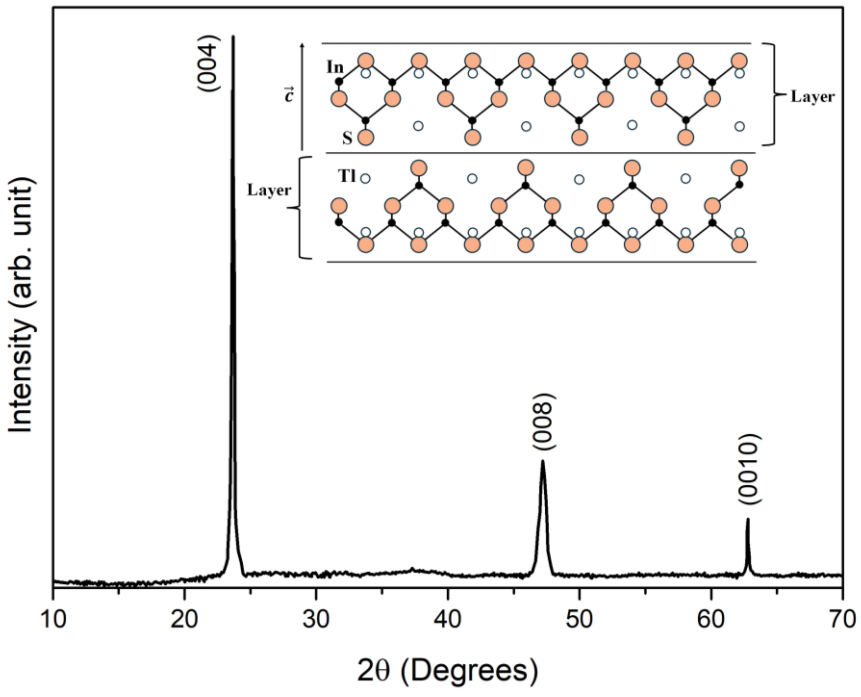

Figure 1. XRD pattern of TlInSSe crystal. Inset indicates the crystal structure of the $TlInS_2$.

3.2. Linear optical characterization

The linear absorption spectra of TlInSSe and $Tl_2In_2S_3Se$ crystals are given in Figure 2(a) and Figure 2(c). As seen in the figures, wide absorption bands occurred between 600 and 1100 nm due to the existence of defect states within the band gap of the crystals. Accordingly, it can be said that the defect states narrow the band gap. Further, the electronic transitions between the valence and the conduction bands correspond to about 550 nm which represents the absorption edge.

The energy of band gap of a crystal can be expressed through the following equation [59],

$$(\alpha h\nu)^{1/n} = A\left(h\nu - E_g\right) \quad (1)$$

where n is 1/2 for direct transitions, α is the linear absorption coefficient, $h\nu$ is the photon energy, A is a constant in the equation, and E_g is the band gap energy of the crystal. Figure 2(b) and Figure 2(d) indicate the Tauc plot of TlInSSe and $Tl_2In_2S_3Se$ crystals, respectively. The point of intersection between the fit line on the linear part of the curve and $h\nu$ axis corresponds to the direct band gap energies of the crystals, and they were found as 2.2 eV for TlInSSe crystal and 2.22 eV for $Tl_2In_2S_3Se$ crystal. Crystals with direct band gap showed better nonlinear absorption compared to crystals with indirect band gap, which can be explained by a decrease in the refractive index for photon energies below the band gap energy due to saturation of available states by the photo-induced carriers in crystals with indirect band gap. Hence, indirect band gap crystals show saturable absorption at low irradiances and nonlinear absorption at high irradiances, making them ideal materials for optical switching applications, while direct band gap crystals show nonlinear absorption at low irradiances, making them ideal materials for optical limiting applications [60, 61].

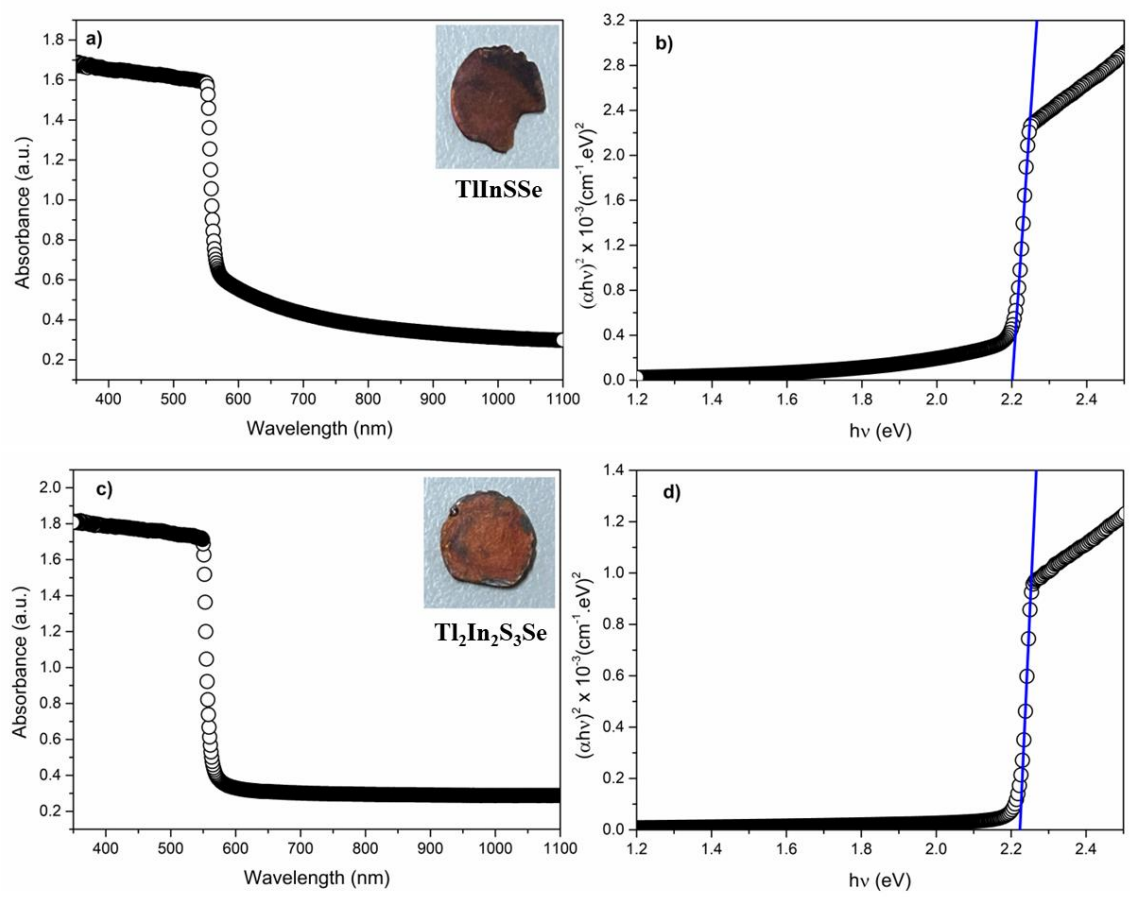

Figure 2. (a, c) Absorption spectra and **(b, d)** Tauc plot of TlInSSe and $Tl_2In_2S_3Se$ crystals.

Mid-gap defects in TlInSSe and $Tl_2In_2S_3Se$ crystals may be based on the Tl, In, S, and Se vacancies. It was reported that the existence of S vacancies provides reduced band gap, enhanced light absorption capacity and carrier density [62, 63]. In the presence of Se vacancies, defect states can occur just below the conduction band and just above the valence band [64]. This makes the band gap of a material relatively suitable for NIR studies.

Defect states that occur in the band structures of semiconductor materials can provide absorption of photons whose energies are lower than that of the band gap by trapping excited electrons. As a result of this, absorptions can occur at lower energy photons than the 2.2 and 2.22 eV, as seen in Figure 2(a). Moreover, defect states can contribute to the NA even lower intensities by trapping electrons excited to higher energy states from valance band. Defect states distribution is determined by the Urbach energy of the crystal that can be obtained through the equation (2) [65] given as

$$\alpha = \alpha_0 \exp\left(h\nu/E_U\right) \quad (2)$$

where α_0 is a constant, and E_U is the Urbach energy. The Urbach energies of TlInSSe and $Tl_2In_2S_3Se$ crystals were obtained as 0.049 and 0.034 eV, respectively, from the inverse slope of the linear part of lnα vs. $h\nu$ curves given in Figure 3. Therefore, it is understood that the defect states are distributed at 0.049 and 0.034 eV below the conduction band of the TlInSSe and $Tl_2In_2S_3Se$ crystals.

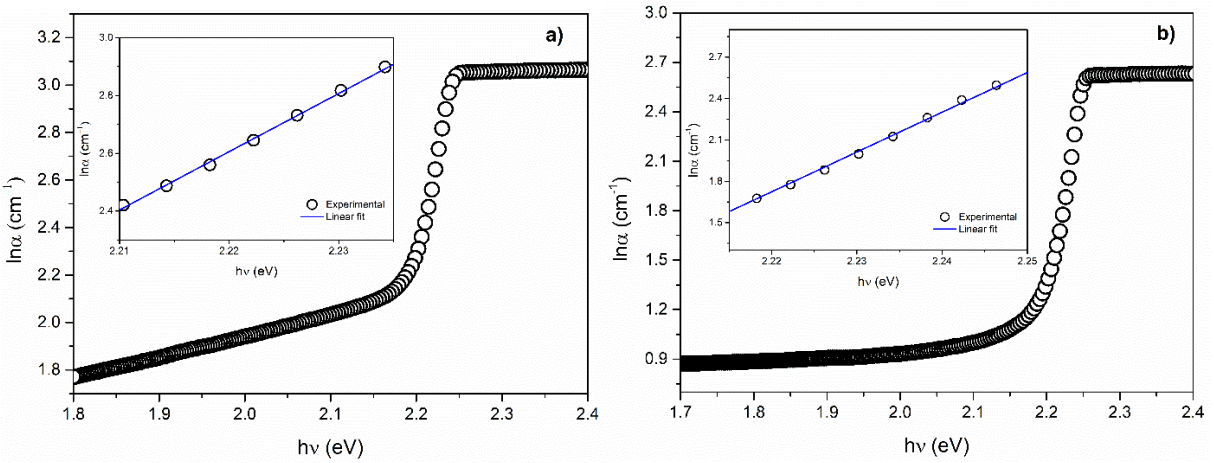

Figure 3. lnα vs. hν plot of **(a)** TlInSSe and **(b)** $Tl_2In_2S_3Se$ crystals.

3.3. Femtosecond transient absorption spectroscopy

The NA mechanisms and decay kinetics of TlInSSe and $Tl_2In_2S_3Se$ crystals were revealed by femtosecond transient absorption spectroscopy. The wavelength of pump light was set at 550 nm corresponding to absorption edge of the studied crystals. In this way, it was possible to excite defect states localized below the conduction band. Transient absorption spectra of TlInSSe and Tl2In2S3Se crystals showed continuous and broad excited state absorption (ESA) bands between 400 and 800 nm (Figure 4). The strength of the ESA signals around 575 nm can be attributed to the transitions from the localized defect states. Also, a red shift of the ESA signal maxima with time delay was observed due to the increasing population of trapped electron by defect states.

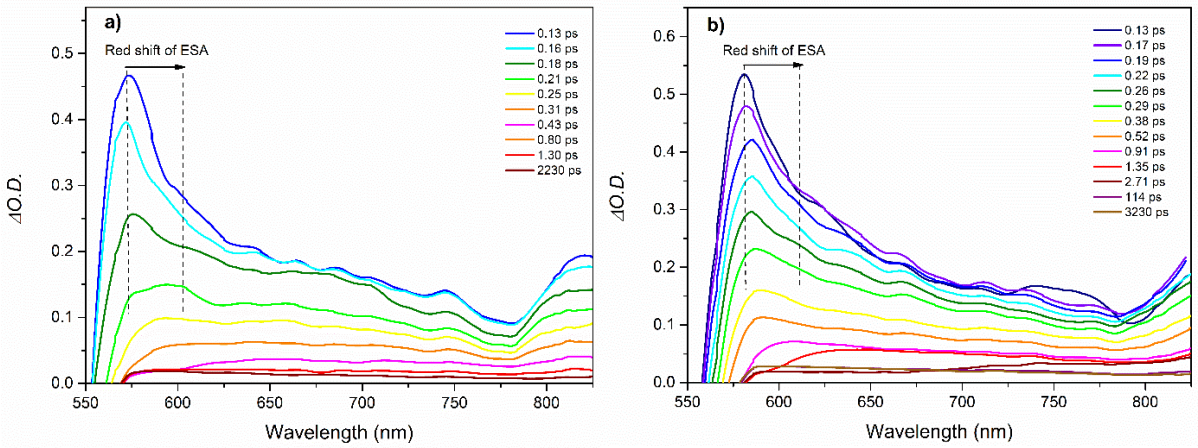

Figure 4. Transient absorption spectra of **(a)** TlInSSe and **(b)** $Tl_2In_2S_3Se$ crystals with 550 nm excitation.

Defect-assisted nonlinear absorption requires pulse duration to be shorter than trapping lifetimes. In this case, trapped electrons can be excited into the conduction band without passing into the valence band. Therefore, since the tapping time of the defect states is higher than the pulse duration of laser source (4 ns), sequential TPA was observed. Moreover, SA properties were also observed at higher intensities due to blocking carriers by the occupation of available states. Accordingly, the decay kinetics were fitted multiexponentially to gain insight into the charge transfer dynamics of the localized defect states. Figure 5 indicates the decay traces of TlInSSe and $Tl_2In_2S_3Se$ crystals by probing 589 and 650/660 nm. In crystals, excited carrier absorptions give rise to transient absorption signals and occur immediately after pump excitation. The fast component below 100 fs suggests that the thermalization process within the conduction band is completed via carrier-carrier scattering of photoexcited carriers. The second time component around 0.12 ps represents the recombination of charges without being trapped by localized defect states. The time components of the TlInSSe crystal are 0.12 ps and 0.5 ps for 589 nm and 650 nm probe wavelength, respectively. The time components of the $Tl_2In_2S_3Se$ crystal are 0.86 ps and 1.18 ps for 589 nm and 660 nm probe wavelengths, respectively. The situation shows that the electrons in defect states localized in the upper energy levels have slower decay compared to the lower energy levels. The slow component, which lies outside the time scale of the pump-probe assembly, represents the loss of carriers after the cooling process, either by recombination at recombination centers or by trapping by local defect states.

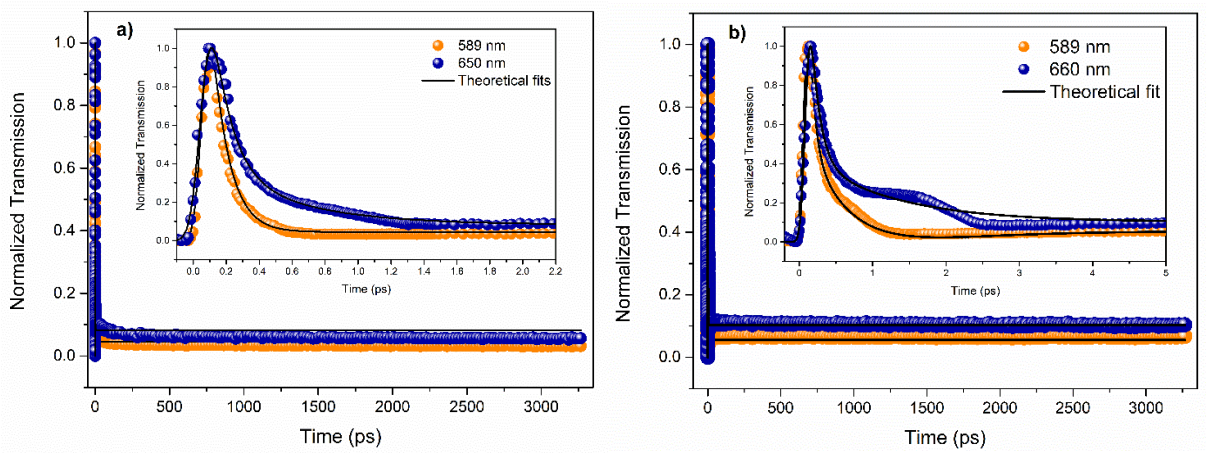

Figure 5. Decay traces of the NA at 550 nm excitation of **(a)** TlInSSe and **(b)** $Tl_2In_2S_3Se$ crystals for 589 nm and 650/660 nm probe wavelengths.

3.4. Nonlinear absorption properties

Nonlinear absorption properties of TlInSSe and $Tl_2In_2S_3Se$ crystals were examined by the OA Z-scan technique at 1064 nm and 4 ns pulsed excitations at various intensities. The OA Z-scan curves were fitted according to two different models. The results of the Z-scan measurements are given in Figure 6.

In model 1 the optical nonlinearity can be defined in the following equations [66],

$$\alpha(I) = \alpha_0 + \beta I \tag{3}$$

where α_0 and β are linear absorption and TPA coefficients, respectively. The transmittance can be given by the Eq. (4),

$$T(z, S=1) = \frac{1}{\sqrt{\pi}\rho_0(z,0)} \int_{-\infty}^{\infty} \ln\left[1 + \rho_0(z,0)e^{-\tau^2}\right] d\tau \tag{4}$$

where $\rho_0(z,0) = \beta I_0 L_{eff}/(1 + z^2/z_0^2)$, z is the position of the material and $z = 0$ at he focus, $z_0 = k\omega_0^2/2$ is the Rayleigh range, ω_0 is the beam waist at focus, I_0 is the intensity of laser beam at the focus, and L_{eff} is the effective thickness of the material and given as $L_{eff} = [1 - e^{-\alpha_0 L}]/\alpha_0$, L is the thickness of the material.

In model 2, to indicate the effects of defect states on the NA, the Z-scan data was also fitted by using a theoretical model which includes the OPA, TPA, FCA, and their saturations given in following equations [67],

$$\frac{dI}{dz'} = -\frac{\alpha I}{1+I/I_{SAT}} - \frac{\beta I^2}{1+I^2/I_{SAT}^2} - \frac{\sigma_0 \Delta N I}{1+I^2/I_{SAT}^2} \tag{5}$$

where I is the output intensity propagates from the crystals, z' is the propagation distance of light inside the crystal, I_{SAT} is the saturation intensity threshold, β is the TPA coefficient, σ_0 is FCA cross-section, and ΔN is a function of α and β.

$$N = \left(\sigma\tau_0/\hbar\omega_0\right) I \tag{6}$$

where τ_0 is the pulse duration of laser and ω_0 is the beam waist at the focus. Therefore, equation (3) becomes the equation (5) as following.

$$\frac{dI}{dz'} = -\frac{\alpha I}{1+I/I_{SAT}} - \frac{\beta_{eff} I^2}{1+I^2/I_{SAT}^2} = -f(I) \tag{7}$$

and

$$\beta_{eff} = \beta + \left(\sigma_0 \alpha \tau_0/\hbar\omega_0\right) \tag{8}$$

where β_{eff} is effective TPA coefficient obtained from the analysis of Z-scan data by model 2.

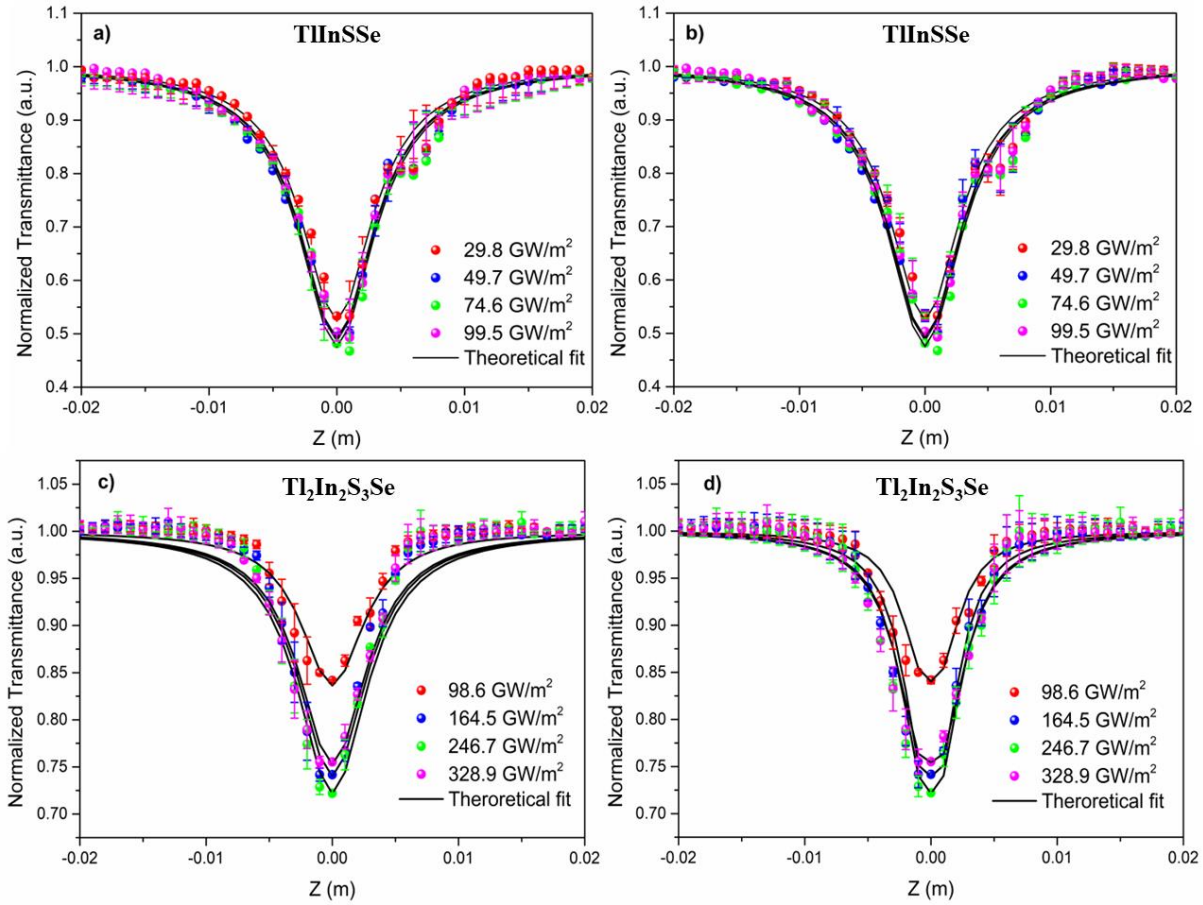

Figure 6. Z-scan data fits of TlInSSe and $Tl_2In_2S_3Se$ crystals performed by using **(a, c)** model 1 and **(b, d)** model 2.

The normalized transmittance of TlInSSe and $Tl_2In_2S_3Se$ crystals decreased with input intensity increasing from 29.8 and 98.6 GW/m^2 to 74.6 and 246.7 GW/m^2, respectively, then it refers to the NA. In general, NA performance depends on factors such as bandgap, laser excitation wavelength, and localized defects. The incident beam energy that is 1.16 eV is higher than half of the band gap energy (E_g > 1.16 eV > E_g/2), and therefore TPA is allowed [68]. Thus, TPA is the main nonlinear absorption mechanism in TlInSSe and $Tl_2In_2S_3Se$ crystals under 1064 nm wavelength excitations. Additionally, it is possible that electrons can be excited to localized defect states at around Urbach energies by OPA. Some of the excited electrons to conduction band may also lose their energy and were trapped by the localized defect states having smaller energy. In addition, the other electrons were excited from defect states to the conduction band by excited state absorption (ESA). This process which includes OPA and ESA is known as sequential TPA. A schematic illustration of the TPA mechanisms is given in Figure 7.

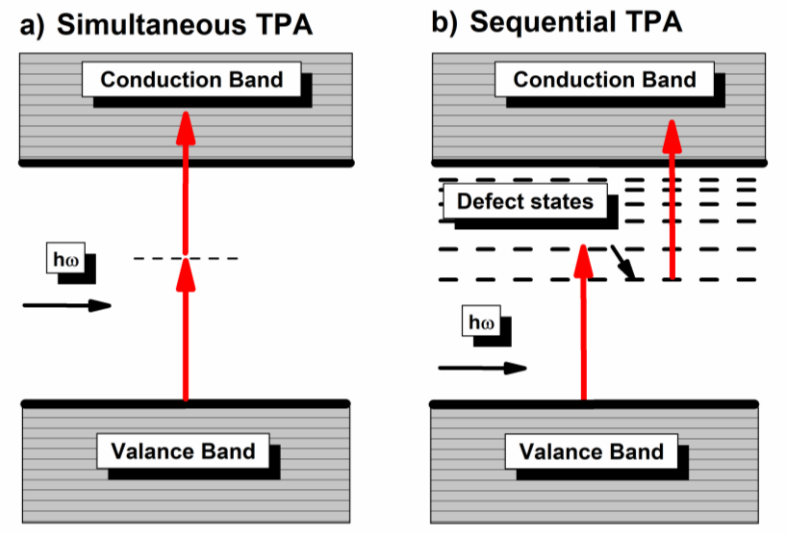

Figure 7. Schematic illustration of the TPA mechanisms.

In order to reveal the contributions of defect states to NA through OPA and ESA mechanisms, open aperture Z scan data were fitted with model 1 and model 2 detailed above. Therefore, the NA coefficients (β) and (β_{eff}) were obtained from the theoretical fits of the Z-scan data by using Eq. (4) and Eq. (5), respectively. Results are listed in Table 1 and Table 2. The β values of TlInSSe crystal decreased from 4.49 x 10^{-10} m/W to 1.58 x 10^{-10} m/W with increasing input intensity from 29.8 GW/m^2 to 99.5 GW/m^2. The β_{eff} also indicated a decrease from 6.05 x 10^{-8} m/W to 1.95 x 10^{-8} m/W while the I_{SAT} increased from 1.13 x 10^{11} W/m^2 to 4.72 x 10^{11} W/m^2 with increasing input intensity. The fact that the β_{eff} values are 100 times higher than the β values reveals that the defect states also contribute to NA through OPA and ESA. The decrease

of β values was also observed in $Tl_2In_2S_3Se$ crystal from 5.62 x 10^{-9} m/W to 2.99 x 10^{-9} m/W with increasing input intensity from 98.6 GW/m^2 to 328.9 GW/m^2. The β_{eff} decreased from 1.51 x 10^{-8} m/W to 8.77 x 10^{-9} m/W while the I_{SAT} increased from 4.23 x 10^{10} W/m^2 to 1.02 x 10^{11} W/m^2 with increasing input intensity from 98.6 GW/m^2 to 328.9 GW/m^2. The fact that the β_{eff} values are higher than the β values reveals that the defect states contribute to NA through OPA and ESA. Intensity dependent SA behaviors were observed as shown in Fig. 6. Saturation occurs if the pulse duration of the light source is shorter than the trapping time of the localized defect states. It supports that the most of electrons are excited to higher energy states and the ground state electrons are depleted at higher light intensities, called ground state bleaching [69, 70]. Additionally, when the appropriate energy levels for electrons to pass through under excitation conditions are occupied, the excitation of more carriers is blocked due to the Pauli exclusion principle and SA is observed [71]. Therefore, filling the localized defect states contributes to SA behavior while the input intensity increases. OPA always contributes to saturation absorption due to the localized defect states since OPA is fluence dependent. When the intensity increases, TPA (simultaneously) and ESA (sequential TPA) will increase and contribute to saturation absorption.

Table 1. Model 1: the β values obtained from the Z scan fit considering only TPA of TlInSSe and $Tl_2In_2S_3Se$ crystals with excitation wavelength (λ_{exc}) and pulse duration (τ).

Materials	λ_{exc}(nm)	τ (ns)	I_0 (GW/m^2)	β (m/W)
TlInSSe	1064	4	29.8	4.49 x 10^{-10}
crystal			49.7	3.24 x 10^{-10}
			74.6	2.28 x 10^{-10}
			99.5	1.58 x 10^{-10}
$Tl_2In_2S_3Se$	1064	4	98.6	5.62 x 10^{-9}
crystal			164.5	6.45 x 10^{-9}
			246.7	4.78 x 10^{-9}
			328.9	2.99 x 10^{-9}

Table 2. Model 2: I_{SAT} and β_{eff} parameters from the Z scan fits considering the defect states of TlInSSe and $Tl_2In_2S_3Se$ crystals with excitation wavelength (λ_{exc}) and pulse duration (τ).

Materials	λ_{exc}(nm)	τ (ns)	I_0 (GW/m^2)	I_{SAT} (W/m^2)	β_{eff} (m/W)
TlInSSe	1064	4	29.8	1.13 x 10^{11}	6.05 x 10^{-8}
Crystal			49.7	1.72 x 10^{11}	4.09 x 10^{-8}

			74.6	2.59 x 10^{11}	2.76 x 10^{-8}
			99.5	4.72 x 10^{11}	1.95 x 10^{-8}
$Tl_2In_2S_3Se$	1064	4	98.6	4.23 x 10^{10}	1.51 x 10^{-8}
Crystal			164.5	5.78 x 10^{10}	1.65 x 10^{-8}
			246.7	8.59 x 10^{10}	1.16 x 10^{-8}
			328.9	1.02 x 10^{11}	8.77 x 10^{-9}

3.5. Optical limiting properties

The optical limiting quality of a material is determined by a threshold that corresponds to a fluence value where the normalized transmittance curve begins to decrease. Therefore, the threshold value must be as low as possible for a high-quality optical limiter. Figure 8 illustrates the normalized transmittance curves as a function of distance-dependent fluence of TlInSSe and $Tl_2In_2S_3Se$ crystals in the near-infrared region.

The distance dependency of the fluence can be determined by the following relation [72],

$$I(z) = \frac{E}{\pi\omega^2(z)t} \quad (9)$$

where E is the energy of incident light per pulse, $\omega(z)$ is the distance dependent beam waist, and t is the pulse duration. $\omega(z)$ can be defined by the relation for Gaussian beam waist [66] given as,

$$\omega^2(z) = \omega_0^2\left(1 + \frac{z^2}{z_R^2}\right) \quad (10)$$

and

$$z_R = \frac{\pi\omega_0^2}{\lambda} \quad (11)$$

where z_R is the Rayleigh distance, ω_0 is the beam waist at focal point, and.λ is the wavelength of the incident light.

The optical limiting threshold of TlInSSe and $Tl_2In_2S_3Se$ crystals was found to be 1.16 and 0.27 mJ/cm^2 at 29.8 and 98.6 GW/m^2 input intensities, respectively. Additionally, a comparison of the results with some reported studies is given in Table 3. A good optical limiter requires as low a limiting threshold as possible. Compared to materials in the crystal, thin film, and glass form in the literature such as $TlGaSe_2$, $TlGaS_2$, InSe, InTe, and $Ge_{20}Te_{75}Bi_5$, $Tl_2In_2S_3Se$ crystal has the best near-infrared limiting threshold in the table. TlInSSe crystal has both relatively low

limiting threshold value. Consequently, TlInSSe and $Tl_2In_2S_3Se$ crystals are promising optical limiter candidates for the near-infrared applications.

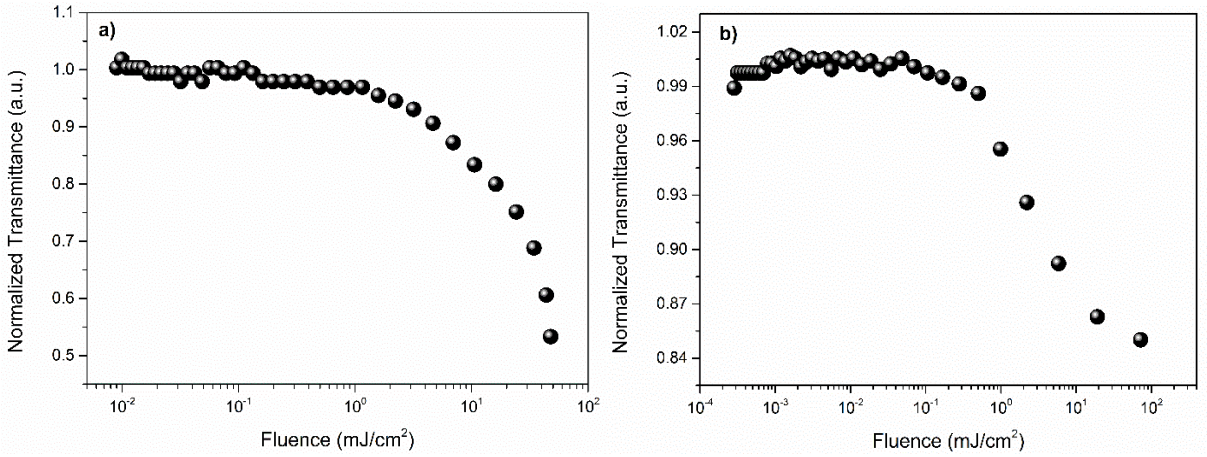

Figure 8. Fluence-dependent nonlinear absorption plots of **(a)** TlInSSe and **(b)** $Tl_2In_2S_3Se$ crystals.

Table 3. Comparison of near-infrared optical limiting threshold values of reported materials.

Materials	λ_{exc}(nm)	Thresholds (mJ/cm^2)	References
TlInSSe	1064	1.16	Present
$Tl_2In_2S_3Se$		0.27	work
$TlGaSe_2$	1064	0.38	[26]
$TlGaS_2$		0.54	
InTe	1064	2.58	[37]
InTe:Er		1.16	
$Bi_{12}TiO_{20}$	1064	5.45	[73]
$Ge_{20}Te_{75}Bi_5$	800	12	[74]
Al-doped InSe	1064	19	[75]
Bi_2Te_3/rGO-PVA	1064	520	[76]

4. CONCLUSIONS

The NA properties of TlInSSe and $Tl_2In_2S_3Se$ crystals were investigated under near-infrared excitations (1064 nm) via OA Z-scan measurements at various light intensities. The lifetime of localized defect states was found to be 8 ns, which is higher than the 4 ns pulse duration, by femtosecond transient absorption spectroscopy. TPA is the main absorption mechanism in the observed NA. Band gap energies are around 2.2 eV allow these crystals to indicate TPA under

near-infrared wavelength excitations (1.16 eV). On the other hand, when the NA contribution of the defect states was taken into account, it was determined that the NA absorption coefficients increased 100 times. This indicates that electrons retained in the defect state by OPA contribute to NA via ESA (sequential TPA). In this way, TlInSSe and $Tl_2In_2S_3Se$ crystals have better absorbing properties at high light intensities. It was observed that the examined crystals showed SA behavior as the intensity increased. This suggests that in addition to the major contribution of TPA to the observed SA, there is also a significant contribution of sequential TPA. The NA behavior of TlInSSe and $Tl_2In_2S_3Se$ crystals enables them to be optical limiting materials in the near infrared region. The optical limiting thresholds of TlInSSe and $Tl_2In_2S_3Se$ crystals were found to be 1.16 mJ/cm^2 and 0.27 mJ/cm^2 at input intensities of 29.8 GW/m^2 and 98.6 GW/m^2, respectively. These values are quite promising when compared to the literature. TlInSSe and $Tl_2In_2S_3Se$ crystals have an advantage in terms of application area diversity, thanks to their NA and SA properties. NA properties provide these crystals with potential for near-infrared optical limiting applications. Additionally, SA properties may make these materials suitable for optical switching applications in optoelectronic devices.

REFERENCES

(1) Ke, D.; Zang, Z. G.; Zhang, Y. J.; Zheng, Y. T.; Zhang, Y. B., The suppressing of excitonic effects in Cu-chalcogenides for solar cell applications. *Sol Energy* **2022,** 247, 255-260.

(2) Tan, J. W.; Zhang, X.; Suh, J.; Ha, N.; Lee, J. W.; Tilley, S. D.; Yang, W. S., Molecular ink-derived chalcogenide thin films: Solution-phase mechanisms and solar energy conversion applications. *Mater Today Energy* **2023,** 34.

(3) Rajabathar, J. R.; Al-lohedan, H. A.; Arunachalam, P.; Issa, Z. A.; Gnanamani, M. K.; Appaturi, J. N.; Ibrahim, S. N.; Dahan, W. M., Synthesis and characterization of metal chalcogenide modified graphene oxide sandwiched manganese oxide nanofibers on nickel foam electrodes for high performance supercapacitor applications. *J Alloy Compd* **2021,** 850.

(4) Le Coq, D.; Boussard-Pledel, C.; Fonteneau, G.; Pain, T.; Bureau, B.; Adam, J. L., Chalcogenide double index fibers: fabrication, design, and application as a chemical sensor. *Mater Res Bull* **2003,** 38, (13), 1745-1754.

(5) Yang, Y. T.; Ge, K. X.; Tao, P.; Dai, S. X.; Wang, X. S.; Zhang, W.; Xu, T. F.; Wang, Y.; Lin, T. J.; Zhang, P. Q., Mid-infrared evanescent wave sensor based on side-polished chalcogenide fiber. *Ceram Int* **2023,** 49, (1), 1291-1297.

(6) Wang, Y. F.; Chen, W. W.; Wang, P. J.; Dai, S. X.; Li, J.; Li, Y.; Fu, Q.; Dai, T. G.; Yu, H.; Yang, J. Y., Ultra-high-power-confinement-factor integrated mid-infrared gas sensor based on the suspended slot chalcogenide glass waveguide. *Sensor Actuat B-Chem* **2021,** 347.

(7) Tintu, R.; Nampoori, V. P. N.; Radhakrishnan, P.; Thomas, S., Nanocomposite thin films of Ga5Sb10Ge25Se60 chalcogenide glass for optical limiting applications. *Opt Mater* **2011,** 33, (8), 1221-1225.

(8) Jun, S. K.; Seo, S.; Park, S.; Kim, T. H.; Lee, M. K. Y.; Hong, S. M.; Kim, T.; Chung, S. M.; Lee, T. Y.; Kim, M.; Kim, H., Amorphous Ge-Se-S chalcogenide alloys via post plasma sulfurization of atomic layer deposition GeSe for ovonic threshold switch applications. *J Alloy Compd* **2023,** 947.

(9) Park, H.; Kumar, R. S.; Akande, A.; Sanvito, S.; El-Mellouhi, F., The rise of Nb-, Ta-, and Bi-based oxides/chalcogenides for photocatalytic applications. *Int J Hydrogen Energ* **2022,** 47, (5), 3358-3370.

(10) Zhang, X. K.; Peng, N.; Liu, T. T.; Zheng, R. T.; Xia, M. T.; Yu, H. X.; Chen, S.; Shui, M.; Shu, J., Review on niobium-based chalcogenides for electrochemical energy storage devices: Application and progress. *Nano Energy* **2019,** 65.

(11) Lee, J. H.; Kim, H.; Yoon, I. J.; Lee, J. I.; Ko, S. Y.; Choi, Y. G., Influence of oxygen incorporation on infrared transmission of ternary Ge-Sb-Se chalcogenide glass in the compositional range for use in infrared-imaging applications. *Ceram Int* **2021,** 47, (24), 34633-34638.

(12) Mersal, G. A. M.; Alkhaldi, H.; Mustafa, G. M.; Mahmood, Q.; Mera, A.; Bouzgarrou, S.; Badawi, A.; Shaltout, A. A.; Boman, J.; Amin, M. A., Study of half metallic ferromagnetism and thermoelectric properties of spinel chalcogenides BaCr2X4 (X 1/4 S, Se, Te) for spintronic and energy harvesting. *J Mater Res Technol* **2022,** 18, 2831-2841.

(13) Su, H.; Jiang, J.; Song, S. J.; An, B. H.; Li, N.; Gao, Y. Q.; Ge, L., Recent progress on design and applications of transition metal chalcogenide-associated electrocatalysts for the overall water splitting. *Chinese J Catal* **2023,** 44, 7-49.

(14) Zhang, J. W.; Guan, Y. N.; Xia, K. L.; Jia, G.; Gu, J. R.; Yang, Z. Y.; Liu, Z. J.; Shen, X., Mechanical properties of SPS sintered chalcogenide glass-ceramics with externally doped crystals. *Ceram Int* **2023,** 49, (5), 8032-8038.

(15) Van, L. C.; Xuan, K. D.; Le Canh, T.; Doan, T. T.; Thi, T. N.; Van Le, H.; Hoang, V., Supercontinuum generation in chalcogenide photonic crystal fiber infiltrated with liquid. *Opt Mater* **2023,** 137.

(16) Zhou, W. F.; Wu, J. J.; Liu, W. L.; Guo, S. P., Ag-based chalcogenides and derivatives as promising infrared nonlinear optical materials. *Coordin Chem Rev* **2023,** 477.

(17) Liang, F.; Kang, L.; Lin, Z. S.; Wu, Y. C., Mid-Infrared Nonlinear Optical Materials Based on Metal Chalcogenides: Structure-Property Relationship. *Cryst Growth Des* **2017,** 17, (4), 2254-2289.

(18) Abdel-Wahab, F.; Ashraf, I. M.; Shaltout, A. A.; Badawi, A.; Ahmed, S. I.; Hassan, M. E., Ellipsometric study of the optical properties of TlInSeS layered crystal. *Opt Mater* **2021,** 114.

(19) Isik, M.; Karatay, A.; Gasanly, N. M., Structural and optical characteristics of thermally evaporated TlGaSe thin films. *Opt Mater* **2022,** 124.
(20) Isik, M.; Karatay, A.; Ech-Chergui, A. N.; Gasanly, N. M., Study of the structural and optical properties of thallium gallium disulfide (TlGaS) thin films grown via thermal evaporation. *Phys. Scripta.* **2022,** 97, (7).
(21) Yuksek, N. S.; Gasanly, N. M.; Aydinli, A., Anharmonic line shift and linewidth of the Raman modes in TlInS layered crystals. *J Raman Spectrosc* **2004,** 35, (1), 55-60.
(22) Odrinskii, A. P.; Seyidov, M. H. Y.; Suleymanov, R. A.; Mammadov, T. G.; Aliyeva, V. B., Photovoltaic currents and activity of structural defects in a ferroelectric-semiconductor TlInS: La single crystal. *Phys Solid State+* **2016,** 58, (4), 716-722.
(23) Nagat, A. T.; Hussien, S. A.; Ebnalwaled, A. A.; Alharbi, S. R.; AlGarni, S. E.; Alkahtani, L. A., Current controlled negative resistance with memory in some binary thallium chalcogenied semiconductor compound. *Journal of Mechatronics* **2015,** 3, 1-9.
(24) Gökçe, S. G.; Mammadov, T. I.; Najafov, A.; Mikailzade, F.; Seyidov, M. Y., Synthesis and magnetic characterizations of TlInFeS solid solution with =0.016 as a new low - dimensional dilute magnetic - semiconductor material. *J Magn Magn Mater* **2022,** 550.
(25) Allakhverdiev, K. R., Two-photon absorption in layered TlGaSe, TlInS, TlGaS and GaSe crystals. *Solid State Commun* **1999,** 111, (5), 253-257.
(26) Ünlü, B. A.; Karatay, A.; Yildiz, E. A.; Dinçbay, T.; Ünver, H.; Gasanly, N.; Elmali, A., Defect assisted nonlinear absorption and optical limiting in amorphous TlGaSSe ($0 \leq x \leq 1$) thin films. *J Lumin* **2022,** 241.
(27) Ünlü, B. A.; Karatay, A.; Yüksek, M.; Ünver, H.; Gasanly, N.; Elmali, A., The effect of Ga/In ratio and annealing temperature on the nonlinear absorption behaviors in amorphous TlGaInS ($0 \leq x \leq 1$) chalcogenide thin films. *Opt Laser Technol* **2020,** 128.
(28) Omar, A.; Qasrawi, A. F.; Gasanly, N. M., Temperature effects on the structural and optical properties of the TlInSe2xS2(1-x) mixed crystals (x=0.3). *J Alloy Compd* **2017,** 724, 98-102.
(29) Isik, M.; Guler, I.; Gasanly, N., Exploring the linear and nonlinear optical behavior of (TlInS2)0.75(TlInSe2)0.25: Insights from ellipsometry measurements. *Physica B: Condensed Matter* **2023,** 669, 415294.
(30) Xie, Y.; Fan, J. D.; Liu, C.; Chi, S. M.; Wang, Z. Y.; Yu, H. H.; Zhang, H. J.; Mai, Y. H.; Wang, J. Y., Giant Two-Photon Absorption in Mixed Halide Perovskite CH3NH3Pb0.75Sn0.25I3 Thin Films and Application to Photodetection at Optical Communication Wavelengths. *Adv. Opt. Mater.* **2018,** 6, (3).
(31) Cai, E. L.; Xu, J. Y.; Xia, Y. Y.; Hao, L. H.; Zhang, Q. Y.; Zhang, S. Y.; Teng, L. H.; Lou, F.; Wang, M. R.; Wang, X.; Wang, A. F.; Li, T., The nonlinear optical properties of Zirconium pentatelluride and its application in ultrafast solid-state lasers. *Opt Laser Technol* **2022,** 150.
(32) Guo, P. L.; An, M. Q.; Shu, Y. Q.; Peng, X. L.; Han, Y. H.; Hu, H. G.; Chen, W. C.; Zhao, Y.; Li, X. H.; Li, J. Q., Nonlinear photonics device based on double perovskite oxide Ba2LaTaO6 for ultrafast laser generation. *Opt Laser Technol* **2022,** 155.
(33) Fu, Y.; Liang, F.; He, C.; Yu, H. H.; Zhang, H. J.; Chen, Y. F., Photon-phonon collaboratively pumped laser. *Nat Commun* **2023,** 14, (1).
(34) Chen, F. F.; Wang, L. J.; Wang, X. L.; Cheng, X. F.; Yu, F. P.; Wang, Z. P.; Zhao, X., Single crystal growth and nonlinear optical properties of Nd3+ doped STGS crystal for self-frequency-doubling application. *Opt Mater* **2017,** 73, 33-37.
(35) Krishna, V. S. G.; Maidur, S. R.; Patil, P. S.; Mahesha, M. G., Role of copper dopant in two-photon absorption and nonlinear optical properties of sprayed ZnS thin films for optical limiting applications. *Phys Lett A* **2021,** 398.
(36) Lee, K.; Lee, I. H.; Khim, Y. G.; Kwon, S. Y.; Lim, G.; Jung, J.; Chang, Y. J.; Lee, J. H., Nonlinear optical properties of PVD-grown Cr2Te3 film and its nonlinear switching application. *J Alloy Compd* **2023,** 956.
(37) Unlu, B. A.; Karatay, A.; Avci, E.; Yildiz, E. A.; Ates, A.; Elmali, A., Above bandgap one-photon excitation induced nonlinear absorption behavior of InTe. *J Lumin* **2022,** 248.

(38) Pepe, Y.; Isik, M.; Karatay, A.; Gasanly, N.; Elmali, A., Nonlinear optical absorption characteristics of PbMoO single crystal for optical limiter applications. *Opt Mater* **2022,** 133.
(39) Pepe, Y.; Isik, M.; Karatay, A.; Yildiz, E. A.; Gasanly, N.; Elmali, A., The role of defects on the transition from saturable absorption to nonlinear absorption of BiGeO single crystal under increasing laser excitation. *J Lumin* **2022,** 251.
(40) Meng, X. X.; Hong, L.; Jiang, Y. H.; Liu, D. J.; Hua, J. L.; Wang, Y. C., Thiophene-modified donor-z-acceptor compound with an enhanced two-photon absorption response: An ultrafast dynamics study. *J Lumin* **2023,** 263.
(41) Karatay, A.; Küçüköz, B.; Çankaya, G.; Ates, A.; Elmali, A., The effect of Se/Te ratio on transient absorption behavior and nonlinear absorption properties of CuInGa(SeTe) ($0 \leq x \leq 1$) amorphous semiconductor thin films. *Opt Mater* **2017,** 73, 20-24.
(42) Karatay, A.; Yuksek, M.; Ertap, H.; Mak, A. K.; Karabulut, M.; Elmali, A., Influence of boron concentration on nonlinear absorption and ultrafast dynamics in GaSe crystals. *Optical Materials* **2016,** 60, 74-80.
(43) Ünlü, B. A.; Sener, D.; Tekin, S.; Yildiz, E. A.; Karatay, A.; Serin, T.; Elmali, A., Enhancement of Nonlinear Absorption in Defect Controlled ZnO Polycrystalline Thin Films by Means of Co-Doping. *Phys Status Solidi B* **2021,** 258, (6).
(44) Karatay, A., Influence of Doping Atoms on Nonlinear Absorption, Ultrafast Dynamics and SHG Behaviors in GaSe. *J Polytech* **2020,** 23, (3), 841-848.
(45) Karatay, A., Controlling of two photon absorption properties by altering composition ratio of GaSSe crystals. *Opt Laser Technol* **2019,** 111, 6-10.
(46) Ertap, H.; Yuksek, M.; Karatay, A.; Elmali, A.; Karabulut, M., Linear and nonlinear absorption, SHG and photobleaching behaviors of Dy doped GaSe single crystal. *Chinese J Phys* **2019,** 59, 465-472.
(47) Liu, K.; Li, Z. G.; Wu, X. Z.; Fang, Y.; Zhou, W. F.; Yang, J. Y.; Sun, Y. F.; Niu, R. P.; Shao, Z. Y.; Chen, L.; Zhao, R.; Song, Y. L., Impact of aluminum doping on nonlinear absorption and ultrafast carriers dynamics of Al:CdO thin films. *Opt Laser Technol* **2023,** 157.
(48) Zhao, R.; Qiu, J. F.; Sun, S.; Sui, Z. Q.; Yang, F. H.; Zhang, H. N.; Zhao, X., The nonlinear optical property of germanium saturable absorber and its application in normal dispersion Er-doped fiber laser. *Infrared Phys Techn* **2022,** 127.
(49) Chakaravarthy, R.; Tao, J.; Liu, C.; Liu, Y.; Ren, W.; Vizhi, R. E., Potassium trihydrogen dioxalate dihydrate (KTO) nonlinear optical (NLO) single crystal for optical limiting application. *Results Phys* **2023,** 51.
(50) Jabber, W. H.; Hassan, Q. M. A.; Al-Saymari, F. A., Evaluation of surface roughness, linear and nonlinear optical parameters of a mixture of sudan black b and polymer films for optical limiting application. *Optik* **2023,** 283.
(51) Gao, L. J.; Li, B. Y.; Yi, H. Y.; Wang, Z. Q.; Shan, T. H.; Song, Y. L.; Zhou, L. M.; Qu, X. W.; Fang, S. M., Nonlinear optical, optical limiting and structural properties of tetrastyryl derivatives with pyrene and bithiophene. *Opt Mater* **2023,** 137.
(52) Pepe, Y.; Yildiz, E. A.; Isik, M.; Karatay, A.; Gasanly, N.; Elmali, A., Tunable nonlinear absorption and optical limiting behavior of NaBi(MoWO) single crystals with ratio of Molybdenum/Tungsten. *Phys. Scripta.* **2023,** 98, (7).
(53) Sahoo, D.; Naik, R., A review on the linear/nonlinear optical properties of Se doped chalcogenide thin films as potential optoelectronic applications. *J Non-Cryst Solids* **2022,** 597.
(54) Lu, X. S.; Li, J. H.; Yang, L.; Zhang, R. N.; Zhang, Y. D.; Ren, J.; Galca, A. C.; Secu, M.; Farrell, G.; Wang, P. F., Third-order optical nonlinearity properties of CdCl2-modifed Ge-Sb-S chalcogenide glasses. *J Non-Cryst Solids* **2020,** 528.
(55) Xing, W. H.; Wang, N. Z.; Iyer, A. K.; Yin, W. L.; Lin, Z. S.; Yao, J. Y.; Kang, B.; Mar, A., Evaluation of nonlinear optical properties of quaternary chalcogenide halides Ba4Si3Se9Br2 and Ba4Ge3Se9Br2. *J Alloy Compd* **2020,** 846.
(56) Guler, I.; Isik, M.; Gasanly, N., Optical characterization of (TlInS2)(0.5)(TlInSe2)(0.5) crystal by ellipsometry: linear and optical constants for optoelectronic devices. *J Mater Sci-Mater El* **2023,** 34, (17).

(57) Gasanly, N. M.; Guler, I.; Goksen, K., Specific features of the optical spectra in TlInSSe layered single crystals. *Cryst Res Technol* **2007,** 42, (6), 621-625.
(58) Sheleg, A. U.; Hurtavy, V. G.; Shautsova, V. V.; Aliev, V. A., X-ray diffraction study of the crystallographic characteristics of TlInSSe solid solutions. *Crystallogr Rep+* **2014,** 59, (2), 186-189.
(59) Tauc, J., Optical properties and electronic structure of amorphous Ge and Si. *Mater Res Bull* **1968,** 3, (1), 37–46.
(60) Gaur, A.; Sharma, D. K.; Ahlawat, D. S.; Singh, N., Optical nonlinearities in direct and indirect band gap crystals on the Z-scan technique with nanosecond laser. *Solid State Commun* **2007,** 141, (8), 445-448.
(61) Sharma, D.; Gaur, P.; Pal Malik, B.; Singh, N.; Gaur, A., Intensity Dependent Nonlinear Absorption in Direct and Indirect Band Gap Crystals under Nano and Picosecond Z-Scan. *Optics and Photonics Journal* **2012,** 2, 98-104.
(62) Sun, X.; Luo, X.; Zhang, X. D.; Xie, J. F.; Jin, S.; Wang, H.; Zheng, X. S.; Wu, X. J.; Xie, Y., Enhanced Superoxide Generation on Defective Surfaces for Selective Photooxidation. *J Am Chem Soc* **2019,** 141, (9), 3797-3801.
(63) Feng, X.; Zhou, S.; Liu, J.; Wu, J.; Wang, J.; Zhang, W.; Jiang, Y.; Liu, Y.; Zhang, J.; Lu, X., Indium oxide-based Z-scheme hollow core-shell heterostructure with rich sulfur-vacancy for highly efficient light-driven splitting of water to produce clean energy. *J Colloid Interface Sci* **2024,** 672, 401-414.
(64) Xiao, K. J.; Carvalho, A.; Neto, A. H. C., Defects and oxidation resilience in InSe. *Physical Review B* **2017,** 96, (5).
(65) Urbach, F., The Long-Wavelength Edge of Photographic Sensitivity and of the Electronic Absorption of Solids. *Phys Rev* **1953,** 92, (5), 1324-1324.
(66) Sheikbahae, M.; Said, A. A.; Wei, T. H.; Hagan, D. J.; Vanstryland, E. W., Sensitive Measurement of Optical Nonlinearities Using a Single Beam. *Ieee J Quantum Elect* **1990,** 26, (4), 760-769.
(67) Yüksek, M.; Kürüm, U.; Yaglioglu, H. G.; Elmali, A.; Ates, A., Nonlinear and saturable absorption characteristics of amorphous InSe thin films. *J Appl Phys* **2010,** 107, (3).
(68) Van Stryland, E. W.; Woodall, M. A.; Vanherzeele, H.; Soileau, M. J., Energy band-gap dependence of two-photon absorption. *Opt Lett* **1985,** 10, (10), 490-2.
(69) Kürüm;, U.; Yüksek;, M.; Yaglioglu;, H. G.; Elmali;, A.; Ateş;, A.; Karabulut;, M.; Mamedov, G. M., The effect of thickness and/or doping on the nonlinear and saturable absorption behaviors in amorphous GaSe thin films. *J Appl Phys* **2010,** 108, 063102.
(70) Ayana, A.; Gummagol, N. B.; Patil, P. S.; Goutam, U. K.; Sharma, P.; Rajendra, B. V., A comprehensive investigation of structural and optical properties of the spray coated Nd-doped ZnO. *J Alloy Compd* **2022,** 922.
(71) Stavrou, M.; Stathis, A.; Papadakis, I.; Lyuleeva-Husemann, A.; Koudoumas, E.; Couris, S., Silicon Nanosheets: An Emerging 2D Photonic Material with a Large Transient Nonlinear Optical Response beyond Graphene. *Nanomaterials-Basel* **2022,** 12, (1).
(72) Vanstryland, E. W.; Sheikbahae, M.; Said, A. A.; Hagan, D. J., Characterization of Nonlinear-Optical Absorption and Refraction. *Prog Cryst Growth Ch* **1993,** 27, (3-4), 279-311.
(73) Pepe, Y.; Isik, M.; Karatay, A.; Gasanly, N.; Elmali, A., Wavelength dependence of the nonlinear absorption performance and optical limiting in Bi12TiO20 single crystal. *J Lumin* **2023,** 253.
(74) Gadhwal, R.; Singh, H.; Devi, A.; Kumar, K., Tunable luminescence and nonlinear optical properties of nano colloidal Ge20Te75Bi5 chalcogenide glass. *Opt Laser Technol* **2023,** 157.
(75) Yan, X. Y.; Wu, X. Z.; Fang, Y.; Sun, W. J.; Yao, C. B.; Wang, Y. X.; Zhang, X. R.; Song, Y. L., Ultrafast broadband reverse saturation absorption in Al-doped InSe thin films for optical limiting at visible/near-infrared. *Optical Materials* **2020,** 108.
(76) Liu, D. M.; He, C. Y.; Chen, L.; Li, W. L.; Zu, Y. L., The nonlinear absorption effects and optical limiting properties of BiTe/rGO thin films. *Opt Mater* **2021,** 111.